University of Groningen

BACHELOR RESEARCH PROJECT

Simulating Capillary Force Bridges Using LAMMPS in Ambient and Aqueous-Ambient Conditions: The Influence of Roughness.

Author:
Magdalena Janewska

Supervisors:
Prof. G. Palasantzas
Prof. A. Grubisic-Cabo
MSc R. B. Seraji

Page count:
27

July 11, 2024

Abstract

This study investigated the formation of capillary force bridges between two solid silicon surfaces, due to DI water liquid meniscus (ambient) and nitrogen nanobubbles (aqueous-ambient) under varying roughness (rms) conditions using LAMMPS molecular dynamics simulations. The output capillary force was then compared to its corresponding result from the theoretical models and the experimental values from other studies. The research focused on two geometries: plane-plane (P-P) and sphere-plane (S-P). For theoretical formulas, surface tension was measured to accurately characterize liquid's cohesive properties and its impact on capillary force formation. Due to limited time and a wrong choice of parameters, simulations of the aqueous-ambient conditions were not performed. For ambient conditions, results indicated significant discrepancies between simulated, theoretical, and experimental (AFM) capillary forces, largely attributed to simulation parameter inaccuracies. Under ambient conditions, water's surface tension was vastly overestimated, ranging from 10^1 to 10^2 N/m, compared to the literature value of 71.97 mN/m [1], impacting capillary force magnitudes. Simulated capillary forces ranged from 10^0-10^1 N for plane-plane to 10^3 N for sphere-plane configuration, while theoretical values were in the order of 10^{-6} N. Thus, both approaches overestimated the experimental capillary forces that were in the range of $10^{-7} - 10^{-9}$N[2]. The study found that roughness did not significantly alter capillary forces within the tested range of 0.00 to 1.36 nm of total RMS roughness (sum of two components), aligning with experimental (AFM) data and suggesting a threshold roughness beyond 1.36 nm necessary for the magnitude to decrease. Theoretical models displayed trends partially agreeing with simulated behavior, highlighting their limitations in providing accurate descriptions for varying roughness. In the same roughness range, the plane-plane geometry displayed an increasing step-like behaviour, while the sphere-plane configuration did not show any specific trends. The results of the study emphasize the need for refined simulation parameters and advanced theoretical models (that focus on roughness outside of its surface tension definition) to bridge the gap between theoretical and experimental results, providing more reliable predictions of capillary forces in various conditions.

Acknowledgements

I would like to express my deepest gratitude to my supervisors, Professor George Palasantzas and Professor Antonija Grubisic-Cabo for their support and supervision during the period of my thesis. I would also like to thank my supervising PhD candidate Razieh BakhshandehSeraji for invaluable guidance on the theoretical aspects of my research. Her expertise and encouragement were instrumental in shaping this work.

Contents

1 Introduction

Adhesion forces are one of the fundamental forces that occur at the interfaces of materials and play a crucial role in nano-scale research. They offer a lot of possibilities in various sectors, such as coating techniques or aid in the development of the transport of fluids [3],[4]. However, they can also act as a hindrance, introducing permanent solid friction between small, moving components and, thus, causing damage [2],[5]. Therefore, a thorough investigation and comprehension of the interactions between surfaces at nanoscale separations is a fundamental requirement for almost any nanotechnology-related field.

Accurately analyzing the adhesion force is highly challenging due to the complex nature of the geometrical contributions from the interacting surfaces. Determining the optimal separation distances between real surfaces, where the surface forces change direction, could enhance applications in micro/nanofluidics and micro/nanoelectromechanical (NEMS/MEMS) systems that operate in liquid environments [2]. This is particularly relevant for future energy conversion systems requiring self-controlled motion [6]. As devices continue to miniaturize, the issue of stiction caused by surface forces between micro/nano-components becomes increasingly significant. However, it also presents an opportunity to control motion by manipulating the direction of the force acting between these moving parts [2].

The primary types of adhesion forces between surfaces include van der Waals forces(due to the temporary dipoles), electrostatic forces (electric charges on the surfaces), and capillary forces. Among these, capillary forces play a dominant role in the direction and magnitude of the adhesion force behaviour at the nano-scale in relatively smooth surfaces (roughness [rms] <3nm) [5]. This phenomenon occurs due to their influence on the behaviour of liquid "bridges" that form between surfaces in close proximity [2]. They can occur even at low relative humidities due to adsorbed water layers on samples and the magnitude of its force is highly dependent on the geometry of the bridge itself [5].

Capillary forces are responsible for phenomena such as Capillary Rise. This flow of liquid in narrow spaces occurs due to an interplay between cohesive forces within the liquid and the adhesive forces between the liquid and its surrounding interfaces [7]. In a similar way, when a liquid spans the gap between two solid surfaces, an attractive or repulsive force is created between them. Thus, forming a capillary force bridge in ambient conditions. This force depends on the contact angle of the liquid with the solid and the surface tension of the liquid [2]. A great number of studies, such as Bakhshandehseraji et al [2], Zwol et al [5], and Sedighi et al [8], were performed to study this physical behaviour and investigate whether it can be minimized or controlled. One of the variables that proved to have a significant influence on the adhesive forces is the rms roughness of the samples [5],[2],[8].

Surface roughness can arise from various mechanisms and it is challenging to prevent and control. In the interaction between two bodies, the influence of roughness on adhesion and friction becomes significant when the space between them is minimal (for example

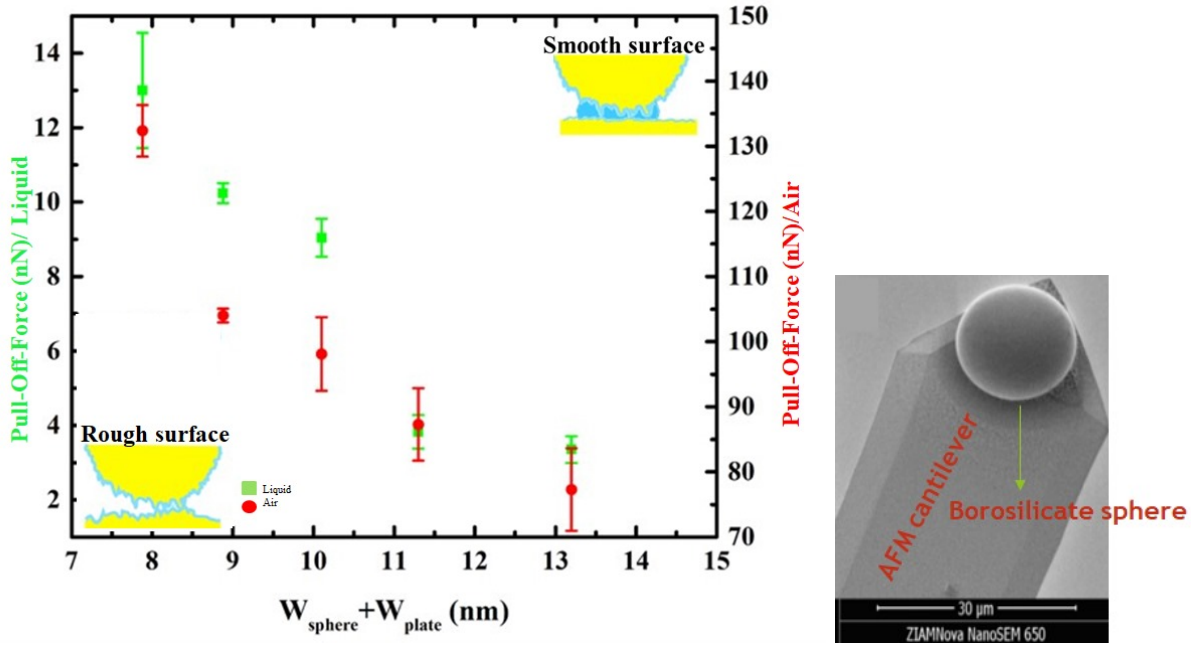

((a)) ((b))

Figure 1: Figures illustrating the results and the AFM tip from the pull-off forces study done by Bakhshandehseraji et al. (a) Pull-off force vs the total rms roughness of Au plate and sphere in ambient (air - right axis) and aqueous (DI water - left axis) conditions. The insets illustrate the capillary bridges for both smooth and rough surfaces in an ambient environment. (b) SEM image of an AFM cantilever from a colloidal-probe technique with a diameter of 20μm. [2]

<100nm) [9]. Current formulas used to describe the forces for this system are only reliable for smooth surfaces. With an increasing height of the asperities, the nonadditivity of the dispersion forces complicates the short-range interactions and breaks the existing models. In recent years, there have been some advances in the theoretical approaches to this issue. Regardless, these solutions still include a considerable number of simplifications. [9]

The established theoretical models suggest the magnitude of capillary force should increase with an increase in roughness [5],[10]. However, due to the aforementioned simplifying assumptions, they do not account for all real-world complexities. For instance, the circular approximation allows for computations of capillary forces between axisymmetric objects, assuming the liquid surface is circular, dominated by surface tension, and negligible gravity. Numerical calculations show this assumption causes less than 5% error for specific angles, but it fails near vapor saturation where Laplace pressure drops [10]. Often neglected factors in calculations also include surface heterogeneity, line tension, microscopic contact angle, and surface deformation [10].

Experimentally, the capillary force can be measured under diverse conditions with a pN to nN sensitivity range by using the AFM force-distance curves between rough surfaces with an uneven shape [2]. Based on research performed by Bakhshandehseraji et al [2],

Zwol et al [5] and Sedighi et al [8], that employed the colloidal probe technique in AFM force measurements, the data showed a promising decreasing trend with an introduction of roughness onto the solid surfaces for the sphere-plane geometry (figure 1(a)). The special AFM probe simulating the geometry can be seen in figure 1(b). In the rough surface regime, the samples are more irregular and uneven compared to the smooth surfaces, which limits the number of interaction points between the surfaces. Consequently, only the highest asperities come into proximity and create capillary-like bridges between them, as shown in the insets of figure 1(a). Accordingly, in the smooth regime, capillary-like bridge formation is more uniform across the interacting surfaces for a greater number of interaction points between the surfaces resulting in increased capillary force (increasing pull-off force) [2]. However, these interactions are reliable only for the sphere-plane geometry, since the plane-plane geometry is significantly less stable in the AFM setting [11]. Therefore, a more in-depth investigation into this variable is required.

The formation of capillary bridges due to liquid meniscus is not the sole origin of this phenomenon. In recent years, nanobubbles (NBs) have been observed to create a capillary-like behaviour in aqueous-ambient conditions between two solid surfaces as well [12]. Nanobubbles can be defined as gas-filled cavities with a diameter of less than 1 μm [12]. Nanobubble technology has applications in various industries, such as environmental technologies for water purification and wastewater treatment, agriculture for improving irrigation and plant growth, and biomedicine for drug delivery and diagnostic imaging. Additionally, NBs are used in food processing to enhance cleaning and sterilization [13].

Contrary to macrobubbles, NBs are very stable and can stay suspended in a liquid for hours or days at a time. This effect occurs due to the Brownian motion, which dominates their behaviour at the nano-scale [12]. This nature allows for the possibility of NBs adhering or nucleating on the solid surface's particles. Further, they seem to contradict the Epstein-Plesset theory due to their high internal pressures [13]. There exist several theories that try to explain this phenomenon. The most popular one argues, that due to the negative charge of pure water, NBs form an electric double layer. Thus, stabilizing their existence with the formation of an ion diffusion layer. Another significant theory suggests that a decreased hydrogen bonding length is responsible for reducing the interfacial gas diffusivity, and hence, making NBs stable [13].

Research has demonstrated a significant difference in capillary forces between air and liquid environments, particularly DI water [2]. To understand this discrepancy, it is essential to examine the formation of capillary bridges in both settings. As shown in figure 2, the adhesion of thin water layers on the edges of hydrophilic surfaces is proportional to the capillary force in the air. Conversely, when two solid surfaces are submerged in a liquid, nanobubbles can migrate and coalesce between them, forming a capillary gas bridge that generates the nanobubble-induced capillary force (NBCF) [2],[12].

To mitigate current limitations in both theoretical and experimental approaches, the

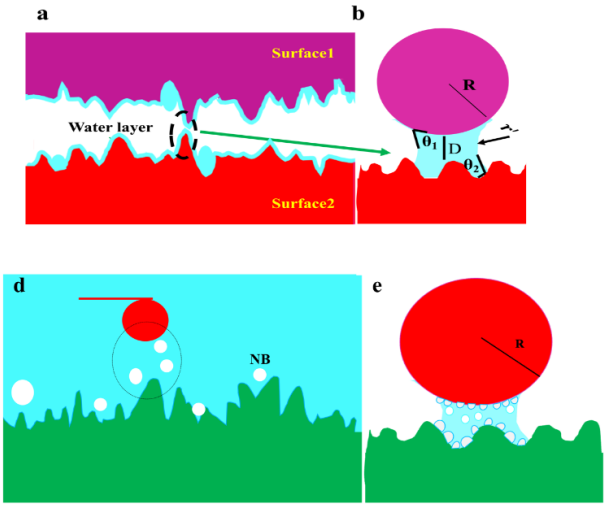

Figure 2: Schematic illustrations of the capillary bridge formation in both ambient and aqueous conditions. (a) Liquid meniscus formed between two asperities due to thin water layers on the rough surface. (b) Sphere-plane geometry in ambient conditions. (d) Nanobubble capillary force (NBCF) bridge formation in an aqueous environment. (e) Sphere-plane geometry for the NBCF bridge. [2]

primary objective of this study is to simulate a simple capillary bridge in both ambient and aqueous-ambient conditions with the use of the molecular dynamics software - LAMMPS. This will involve creating models that accurately represent the interactions and behavior of liquid bridges within two silicon surfaces in these environments. The resulting force from the models will then be compared to theoretical predictions and discussed alongside experimental data (sphere-plane configuration), to investigate the extent to which this phenomenon can be accurately simulated with current technology. Further, the simulations will be performed for two types of geometries: plane-sphere and plane-plane, and then compared. This comparison will help determine whether the geometric configuration of the surfaces affects the behavior of capillary bridges. Another key objective is to analyze how varying the roughness (rms) of silicon surfaces affects the capillary forces and observe whether the trend is decreasing or increasing.

2 Theory

While discussing the capillary forces due to the liquid meniscus bridge formation, it is important to mention two formulas that govern its behaviour: The Young-Laplace formula and the Kelvin equation. The former draws a relation between the curvature of the bridge and the pressure difference between the liquid-gas phases and is written as follows

$$\Delta P = \gamma(\frac{1}{r_1} + \frac{1}{r_2}), \tag{1}$$

where ΔP is the pressure difference, γ is the surface tension of the liquid interface, while r_1 and r_2 are principal radii of curvature (figure 3) [10]. This formula assumes that the gravitation acting on this system is negligible. The latter fundamental equation relates the curvature of the bridge with the vapour pressure and is written as

$$RT \ln \frac{P}{P_0} = \gamma V_m(\frac{1}{r_1} + \frac{1}{r_2}), \tag{2}$$

where R is the ideal gas constant, $\frac{P}{P_0}$ is the relative humidity, V_m is the molar volume of the liquid, and T is the temperature. Rearranging the equation in terms of Kelvin length gives the range of the capillary forces in the form of

$$\lambda_K = \frac{\gamma V_m}{RT}, \tag{3}$$

where λ_K is the Kelvin length. Hence, for a capillary bridge to form, the distance between two solid surfaces should be equal to or less than $2\lambda_K$.[10]

The simplified capillary model for relatively smooth surfaces can be described using the Attard model as a basis. In this model, the capillary force can be divided into two main components. The first component is the surface tension at the gas-liquid-solid contact, while the second is the pressure force caused by the pressure difference [12]. Hence giving the overall equation

$$F_{cap} = F_s + F_p. \tag{4}$$

2.1 Plane-Plane Geometry

The plane-plane system is one of the simpler shapes to model, due to its geometry. However, with current technological limitations, it is also a configuration that cannot be measured experimentally [11]. While formulating the theoretical capillary force model, equations differ depending on whether the bridge originates from the liquid meniscus or the nanobubbles [10],[12]. Therefore, different approaches have to be taken based on the origin of the capillary bridge. For the ambient conditions equation 4 is transformed into

$$F_{cap} = 2\pi r_0 \gamma \cos\theta + \pi r_0^2 \gamma(\frac{1}{r_2} - \frac{1}{r_1}), \tag{5}$$

for $D \leq r_2 c$ and $F_{cap} = 0$ for $D > r_2 c$, where $c = \cos\theta_1 + \cos\theta_2$ and D is the separation distance between two plates [10]. The visualization can be seen in figure 3, where θ

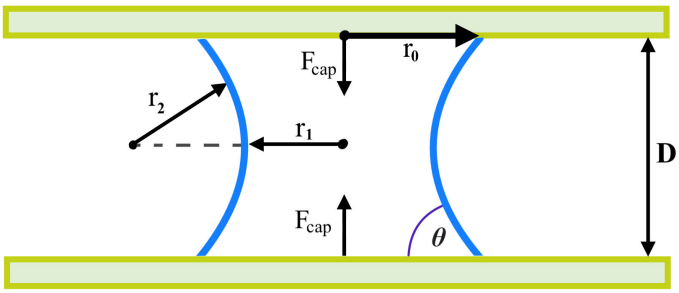

Figure 3: Schematic illustration of the concave capillary force bridge due to the liquid meniscus in the plane-plane configuration.

corresponds to the contact angle between the solid and the liquid, and r_0 is the radius of the bridge region in contact with the solid surface. The radius of the curvature is denoted as r_2, while r_1 is the length from the normal of the bridge to the end of the curvature on the same vertical height as the middle of the curvature circle. Here the first part corresponds to the surface tension component, while the second part to the pressure difference component [10]. For the NB capillary force bridge, the formula is slightly altered to accommodate the switch in the gas-liquid position. Hence giving the expression

$$F_{cap} = -2\pi r_0 \gamma \sin\theta + \pi r_0^2 \gamma (\frac{1}{r_1} - \frac{1}{r_2}). \tag{6}$$

The minus sign in the F_s component appears due to a sign convention, which indicates the direction of the force that is typically opposite to that of the meniscus force [12]. Thus, negative values represent an attractive force, whereas positive values indicate a repulsive relation. As can be seen in figure 3, most of the variables (θ, r_0, r_1, r_2) can be measured off of the bridge's snapshots. Further, both formulas draw the same conclusion, being, that as the contact angle θ between the liquid-solid interface decreases and is below 90°, the capillary force should increase. Further, in the case of CA above 90°, increasing θ will increase the force magnitude as well.

2.2 Plane-Sphere Geometry

The plane-sphere configuration, often analyzed using Atomic Force Microscopy (AFM), presents a different set of equations for capillary forces due to the curved geometry of the sphere interacting with the plane. The capillary force due to liquid meniscus formation can be obtained using the equation

$$F_{cap} = \pi\gamma R[-\sin\phi + (\cos(\theta_1+\phi) + \cos\theta_2) \times \sin\phi^2 (1 - \cos\phi + \frac{D}{R})^{-1}] + 2\pi\gamma R \sin\phi \sin(\theta_1+\phi), \tag{7}$$

where R is the equivalent sphere radius, D is the closest distance between the sphere and the plate, θ_1 is the contact angle of the liquid and the sphere, θ_2 is the contact angle of the liquid and the plane, and ϕ is the filling angle of the sphere (figure4) [5]. This equation is

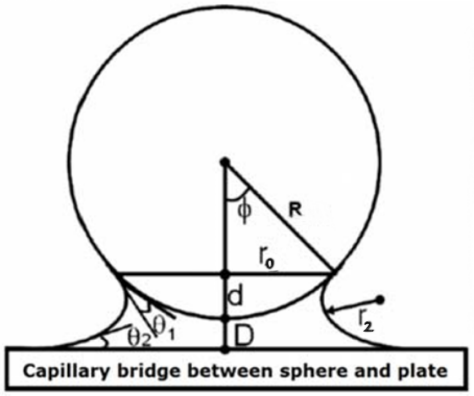

Figure 4: Schematic illustration of the concave capillary force bridge due to liquid meniscus in the sphere-plane configuration. [5]

constructed ignoring the van der Waals forces and modeled for relatively smooth surfaces [5]. A simplified formula is used for $D \ll R$ ($\phi \approx 0°$) [5]. However, for the simulations performed in this report, the values of the filling angle ϕ are not close to 0°, since the size of the sphere is not significantly bigger than the thickness of the capillary bridge.

Based on equation 7, for angles θ or $\phi < 90°$, if the liquid-solid contact angles decrease, the capillary bridge should spread more across the solid surfaces and therefore increase the filling angle ϕ value. Thus, the $-\sin\phi$ term will become more negative, while $\sin^2\phi$ will increase, increasing the overall force. Further, the second term with $\sin\phi\sin(\theta_1+\phi)$ will increase due to the significant contribution from $\sin\phi$. The net capillary force is then expected to increase as ϕ increases with decreasing θ_1 and θ_2. However, the precise change significantly depends on the exact relation between ϕ and the contact angles. This highlights the importance of the interplay between the angles and the curvature in determining the behavior of capillary forces in the sphere-plane configuration.

On the contrary, for angles $\theta > 90°$ and $\phi < 90°$, the capillary force will depend on the exact values of $\theta_1 + \phi$ and the balance between the negative contributions from the first term and the positive or negative contributions from the second term. Generally, if $\theta_1 + \phi$ results in a positive sine term, the force could remain positive or reduced. If it results in a negative sine term, the force could be significantly reduced or change the direction.

Due to the nanobubble capillary forces (NBCF) being a relatively recent discovery, there are no coherent established theoretical models for the sphere-plane geometry. However, similarly to the NBCF in the plane-plane configuration, one could argue that the capillary force still mainly consists of the surface tension and the pressure difference components [2]. Therefore, a decrease in the contact angle between the solid and liquid should lead to an increase in the total force as well.

((a)) ((b))

Figure 5: Microscope images of a liquid drop on (a) hydrophilic and (b) hydrophobic organic surfaces [made during one of the BSc Physics lab courses].

2.3 Roughness

To link the capillary force with the roughness, a discussion of the contact angle (CA) and wettability concepts is required. The former parameter represents the angle the liquid makes with a solid surface, while the latter can be defined as a measure of how easily a liquid spreads across or adheres to that surface [14]. Hydrophobic surfaces tend to exhibit very low wettability, whereas hydrophilic surfaces are characterized by high wettability. Therefore, as the liquid contracts/spreads across the sample, hydrophobic surfaces showcase high CA, while hydrophilic low CA. Typically, a contact angle greater than 90° signifies a hydrophobic surface, while angles less than 90° indicate hydrophilic properties (figure 5) [15]. This phenomenon is reflected in the bridge geometry of the capillary force bridges. In ambient conditions hydrophilic surfaces form concave bridges, while hydrophobic take the shape of a convex bridge. The opposite occurs when the bridge is formed due to gas NBs in an aqueous environment, in which the expected geometries are reversed [12].

Two distinct wetting regimes for textured surfaces can be characterized: homogeneous (Wenzel) and heterogeneous (Cassie-Baxter). In the heterogeneous regime, the air is trapped between the liquid droplet and the surface, while in the homogeneous regime, the surface is entirely submerged in the liquid [15]. In this study, the focus was placed on the homogeneous regime, which can be described using the Wenzel equation

$$\cos\theta_W = r_W \cos\theta_Y, \tag{8}$$

where r_W is the roughness ratio, θ_W is the apparent contact angle the liquid makes with the sample and θ_Y is the ideal Young's contact angle [15]. The roughness ratio is equal to 1 for ideally smooth surfaces, and greater than 1 for rough surfaces [15]. According to this formula, as the ratio r_W increases in value, the CA of the liquid θ_W should increase for angles $> 90°$ and decrease for $< 90°$. For hydrophilic Au samples, this relation is shown in

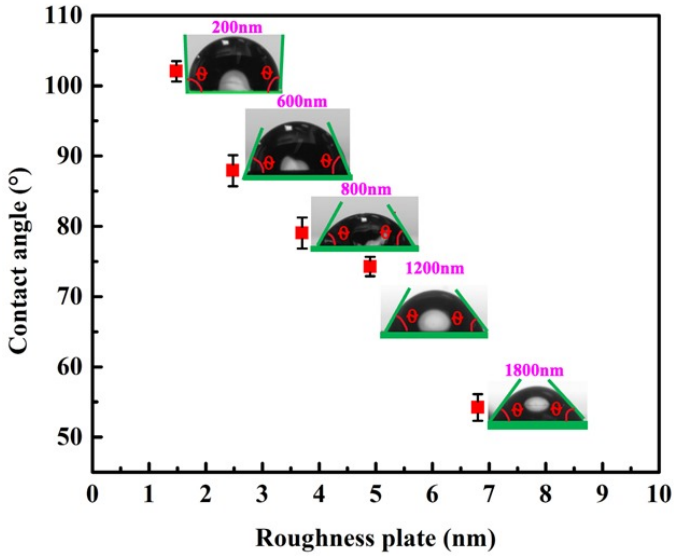

Figure 6: The contact angle of a liquid drop on an Au-coated surface vs rms roughness. [2]

figure 6.

This result can be extended to the capillary force formulas 5-7. Hence, for both hydrophilic and hydrophobic surfaces, an increase in the roughness ratio signifies an increase in the net capillary force. It is worth noting, however, that both the contact angle and the surface tension provide a very limited view of the influence of roughness. Thus, this study employs simplified models of the capillary force for relatively smooth surfaces, that exclude parameters outside of the interplay of cohesive forces acting on a liquid drop.

2.4 Surface Tension of Liquid

The cohesive forces acting on the water droplet and the surface significantly contribute to the magnitude of the contact angle and the capillary force. Since systems naturally strive to reach chemical equilibrium with their environment, they aim to minimize the available Gibbs free energy, which in turn is a monotonically increasing function of the contact angle [14],[16]. Therefore, lower contact angles in the wetting regime are more thermodynamically stable, causing surfaces to minimize this angle as much as possible. This phenomenon can be described using the surface free energy of the substrate, which is the work required to form a unit area of a certain surface and is equivalent to the surface tension in liquids [17].

Using the surface tension property, one can make precise predictions of the liquid-solid interactions. When a liquid's surface tension is lower than the critical surface tension of a solid, the liquid will wet the surface, resulting in a contact angle of 0°. Young's equation describes these interactions as:

$$\gamma_{sv} - \gamma_{sl} = \gamma_{lv} \times \cos\theta, \tag{9}$$

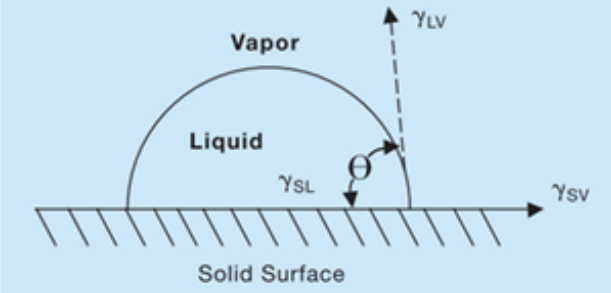

Figure 7: Schematic illustration of cohesive forces acting on a liquid drop on a solid surface. [14]

where γ_{sv} is the critical surface tension of the solid, γ_{sl} is the interfacial surface tension, γ_{lv} is the surface tension of the liquid (figure 7) [14],[18]. In the case of water, its literature surface tension value is around 0.072 N/m [1]. Therefore, a surface with a critical surface tension lower than 0.035 N/m tends to be hydrophobic, while a surface with a critical surface tension higher than 0.045 N/m is regarded as hydrophilic. It occurs due to a relationship between the surface tension of the substrate and the cohesive forces associated with the bulk of water. If the energy increases and is greater than the cohesive forces, the liquid wets the surface more [14]. Silicone's surface tension is in the range of 0.020 up to 0.023 N/m [18]. Therefore, it should appear hydrophobic in the simulations with a convex geometry for ambient conditions and concave for aqueous.

3 Methodology

3.0.1 AFM and Theoretical Models

The topic of capillary force bridges can be studied through several methods. However, as mentioned before, each approach has great limitations due to either equipment or current theoretical formulas. AFM measurements are well suited to measure the adhesion forces in both ambient and aqueous conditions. However, they are only possible for specific geometries (such as sphere-plane) and result in very complex data output [11]. Further, for the NBCF, it is very challenging to obtain images of the capillary bridge and its nanobubbles due to its nanoscopic resolution (sub-10nm). Hence, a capillary model with fitting parameters is required to monitor the shape of the bridge [12]. On the contrary, the theoretical models (especially for the NBCF) are also simple due to the same issue of limited capillary models with fitting parameters [10].

The Molecular Dynamics (MD) approach allows for more possible configurations and for access to various environmental conditions, that are not possible with experimental methods. Further, even though it still operates on certain models, it can help develop more advanced theoretical models by showcasing new additional parameters.

3.1 Molecular Dynamics

To investigate the influence of surface roughness on capillary forces in capillary bridges under ambient (liquid meniscus) and aqueous (nanobubble) conditions, the study employed the aforementioned LAMMPS software. It utilized the pre-built Windows package with an additional Pizza.py toolkit. The visualization of the simulation box was done through Ovito and *.lammpstrj* files from the LAMMPS code. Further, the theoretical analysis of the curvature radiuses, the contact, and filling angles was done with the use of ImageJ and its DropSnake plugin. The theoretical values of the capillary forces in both geometries were obtained with the use of formulas 5-7. The surface tension of the liquid was extracted from the LAMMPS output during the equilibrated runs.

The main components of both environments included pure silicon as the solid, DI water molecules as the liquid, and nitrogen as the gas responsible for NBs. Even though pure silicon is naturally hydrophobic, it was chosen due to its simplicity during modeling [18]. Original solid ideas included Au (can be modified to be hydrophilic) or SiO2 (naturally hydrophilic) [2],[12],[19]. However, their interactions were too complex to model and make work in the given time limit. DI water was selected as the liquid of choice since it's employed most commonly in the experimental studies [2]. In the script, an SPC pre-built molecule model on the LAMMPS website was used with slight modifications to the charges [20]. Further, Nitrogen was employed in the NB simulations, due to its availability in air. Hence, its occurrence in naturally formed NBs in experimental environments, where the bubbles consist of air [13].

	O-O	O-H	H-H	Si-Si	N-N	O-Si	O-N	Si-N
ϵ [kcal/mol]	0.1554	0.0	0.0	49.99989	0.0797	0.6130	0.11129	1.9962
σ [Å]	3.16557	0.0	0.0	2.095	3.614	2.630285	3.389785	2.8545

Table 1: Lennard-Jones model coefficient for all interactions between atoms in the LAMMPS simulation.

RMS roughness was imposed as the outer layer of the silicon plates/sphere. It was constructed using a sine wave generated with a Python script. The amplitude of the function was obtained with the RMS formula [21]

$$R_{rms} = \frac{A}{\sqrt{2}}. \tag{10}$$

The magnitudes of roughness were chosen to be 1.48, 2.45,3.70,4.90, and 6.80 Åto mimic the roughness variation used in the study done by Bakhshandehseraji et al [2]. However, all of the original values were scaled down by an order of 10, due to the total time the code required to be fully processed. With rms roughness values greater than 0.7nm, the total number of molecules in the system increased drastically and therefore the computation time extended well over 12 hours. Each utilized roughness layer contained from 14000 to 16000 molecules.

All molecule interactions were modeled with the use of Lennard-Jones potential. Its equation is the following

$$E = 4\epsilon[(\frac{\sigma}{r})^{12} - (\frac{\sigma}{r})^{6}], \tag{11}$$

where r is the distance between two interacting particles, ϵ is the depth of the potential well, and σ is the distance at which the particle-particle potential energy is equal to zero [20]. The specific simulation parameters can be seen in table 1. All dispersion interactions have a cut-off radius of 10.9 Å. The values for O-O, H-O, and H-H were input according to the SPC molecule model from the LAMMPS database [20]. The rest was determined based on the analysis from a study that similarly employed Si solid and SPC water molecules and another study that focused on exploring the force fields for nitrogen [22],[23]. The former study focused on varying the ϵ_{Si-O}, and it ranged in magnitude from 0.2786 to 0.6130 (kcal/mol) [22]. Thus, the biggest value was taken in the following simulations to account for the greatest potential well depth. The latter study obtained the ϵ_{N-N} and σ_{N-N} values only [23]. Using Lorentz-Berthelot mixing rules, an arithmetic mean for σ_{N-Si} and σ_{N-O}, and a geometric mean for ϵ_{N-Si} and ϵ_{N-O} were employed [20].

As mentioned above, to obtain the theoretical values of the capillary forces, simulated water's surface tension was utilized. It was computed with the use of the Irving Kirkwood model in the form of

$$\gamma = \frac{1}{2}\int_0^{L_x} [P_N(x) - P_T(x)]\, dx, \tag{12}$$

where P_N is the component of pressure acting perpendicular to the surface, while P_T refers to the components of pressure acting parallel to the surface [24].

3.2 Simulations

The LAMMPS input scripts used for this study are detailed below and are explained step-by-step to clarify the simulation setup, parameters, and procedures involved. For both configurations, the simulation was conducted in a 3-dimensional box with a periodic boundary condition to simulate an infinite system. The units were set to "metal" to ensure appropriate units of length/energy/time [20]. Thus, they had to be correctly converted while inputting the values, because the units in the script were in Angstroms/Bars/eV per Å. Since the system required pre-modeled water and N_2 molecules, the atom_style was set to full to allow for the definition of molecules with bonds, angles, and dihedrals.

3.2.1 Ambient Conditions

The size of the simulation box was chosen to be $27.5 \times 27.5 \times 27.5$nm. While trying to run a bigger simulation with a greater number of molecules, the simulations were taking too much time (more than 12 hours). Thus, due to time constraints, the size was decreased. Accordingly, the plate dimensions were set to $22.5 \times 22.5 \times 4$ nm, the sphere radius to 14nm, the distance between the solids to 1nm, and the bridge cylinder radius to 3nm. Trial simulations were run with a smaller Si plate thickness. However, then the silicon plate was less rigid and it led to its atoms detaching from the plate region and causing the loss of the plate shape.

After the regions were defined, the solid silicon was introduced first. Its standard lattice constant was utilized, being a=5.431×10^{-10} m [25]. If needed, an external file was included to apply specific surface roughness to the silicon atoms. The silicon atoms were kept in a rigid configuration to simulate a solid surface. Then, an NVT equilibration (const. atom number, volume, and temp) with a Noose-Hoover thermostat was run. After the Si system reached an equilibrium, the 1234 water molecules were added to the cylinder region in the middle of the solid Si configuration. The harmonic bond/angle styles and their coefficients were used, to be suitable with the SPC water model [20]. The neighbour settings were set to update every new run. The system's energy was minimized in steps of 10^5 eV for energy and 10^{-7} eV/Åfor force, using the conjugate gradient method.

Due to an issue with water molecules "flying off" of the simulation box, the SHAKE algorithm was applied to constrain all water molecules. Then the NVT simulation was carried out at 300K to equilibrate the system with a gradual increase of timesteps. This slow change in timesteps was caused by the system breaking during the simulations with bigger and more sudden timestep changes. After the equilibration, forces acting on the silicon plates and/or half-sphere from the water meniscus and pressure tensor components were computed and exported into appropriate *.txt* files. The equilibrium simulation was

then carried out for an additional 10000 steps for the data collection. The output files contained 100 snapshots and force/pressure values of each equilibrated system.

3.2.2 Ambient-Aqueous Conditions

The attempt at generating a stable NB bridge involved a similar simulation box setup. The size of the simulation, as well as the shapes of the solid silicon components, were modeled to be the same as in ambient conditions to allow for fair comparisons between both environments. However, in the NBCF bridge, the cylinder region was defined for the nitrogen gas instead, while the unoccupied space was designated for DI water molecules (with the use of the *delete_atoms* function).

Similarly to the previous script, the silicon structures were inserted first into the system and the remaining space was filled with the DI water. Then, an NVT simulation was run to equilibrate the environment at 300K. Following, the cylinder region was removed of any water molecules and the nitrogen gas was inserted. The energy of the system was minimized in steps of 10^5 eV for energy and 10^{-7} eV/Åfor force, using the same conjugate gradient method. The NVT simulation was run again for a greater amount of steps and with a gradually increasing timestep. After the equilibrium of the entire system was reached, the simulations were run to again contain 100 snapshots each. Further, the forces acting on the plates/sphere components and the pressure tensors were collected using the same method as in section 3.2.1.

3.3 Data Analysis

For each run, the z-component of force and the pressure components (normal and two tangential) of the output files were averaged and a standard error of the mean was calculated (formula 13). After taking the mean from the force files, the final simulated data results for the capillary forces acting on each plate/sphere were obtained. The pressure values were input into the Irving Kirwood formula and a liquid-gas surface tension was computed. Further, to get the theoretical approximation for each rms and geometry, every second snapshot visualized in Ovito was studied, and values for $r_0, r_1, r_2, \theta, \theta_1, \theta_2, \phi$ were measured using ImageJ analysis. These values were then also averaged and a standard error of the mean was calculated. The variables from ImageJ measurements were assigned a measurement error due to the length/angle selection being done manually by me. The assigned length error was equal to $0.1nm$, while the assigned error of the angle to $0.005°$. These values were included in the error propagation.

		Surface Tension of the DI water [N/m]					
	Roughness [nm]	0.000	0.148	0.245	0.370	0.490	0.680
Plane-Plane		4.3955 $\pm$0.3809 $\times 10^1$	3.6821 $\pm$0.0269 $\times 10^1$	2.3881 $\pm$0.0312 $\times 10^1$	1.0702 $\pm$ 0.0078 $\times 10^2$	1.0317 $\pm$0.0782 $\times 10^2$	1.0353 $\pm$0.0816 $\times 10^2$
Sphere-Plane		2.6614 $\pm$0.0271 $\times 10^1$	2.9022 $\pm$0.0310 $\times 10^1$	2.4901 $\pm$0.0239 $\times 10^2$	2.5086 $\pm$0.02399 $\times 10^1$	2.4776 $\pm$0.0233 $\times 10^1$	2.4534 $\pm$0.0238 $\times 10^1$

Table 2: Final DI water surface tension results for varying rms roughness in both P-P and S-P configurations.

4 Results

All raw data from the simulations was collected and can be seen in the Appendix.

4.1 Ambient Conditions

4.1.1 Water's Surface Tension

After using the standard error and the mean on the pressure tensor data, equation 12 was employed to obtain the final values of the DI water surface tension. The results can be seen in table 2. In figure 8, the data was visualized and compared to the literature value of water's surface tension (71.97 mN/m [1]). All values are in the range of $10^1 - 10^2$ N/m, which is greater by an order of $10^3 - 10^4$ than its literature value. Thus, it suggests an error in the simulations, that further could have influenced the final capillary force results. For the plane-plane (P-P) geometry, the surface tension trend between 0.00 and 0.245 nm rms resembles a logarithmic decrease. However, with greater roughness values, the data rapidly increases by a factor of 10 and remains in the range of 107-103 N/m. On the contrary, the tension values in the sphere-plane (S-P) geometry do not have any significant changes in magnitude across the rms roughnesses and are in the range of 24-29 N/m. At rms 0.245 both configurations agree on the value of the surface tension the most.

4.1.2 Capillary Force Bridge

The snapshots from ImageJ were used in the bridge analysis and the examples can be seen in figures 9-10. For both geometries, the simulated structures resemble a bridge with hydrophilic properties, contrary to the expected hydrophobic nature of silicon. The resulting bridge curvature is pronounced in all runs, indicated by a small curvature radius measured and the contact angles that range from 2 to 20 degrees.

In both configurations, rough layers of silicon, that were not in contact with the liquid

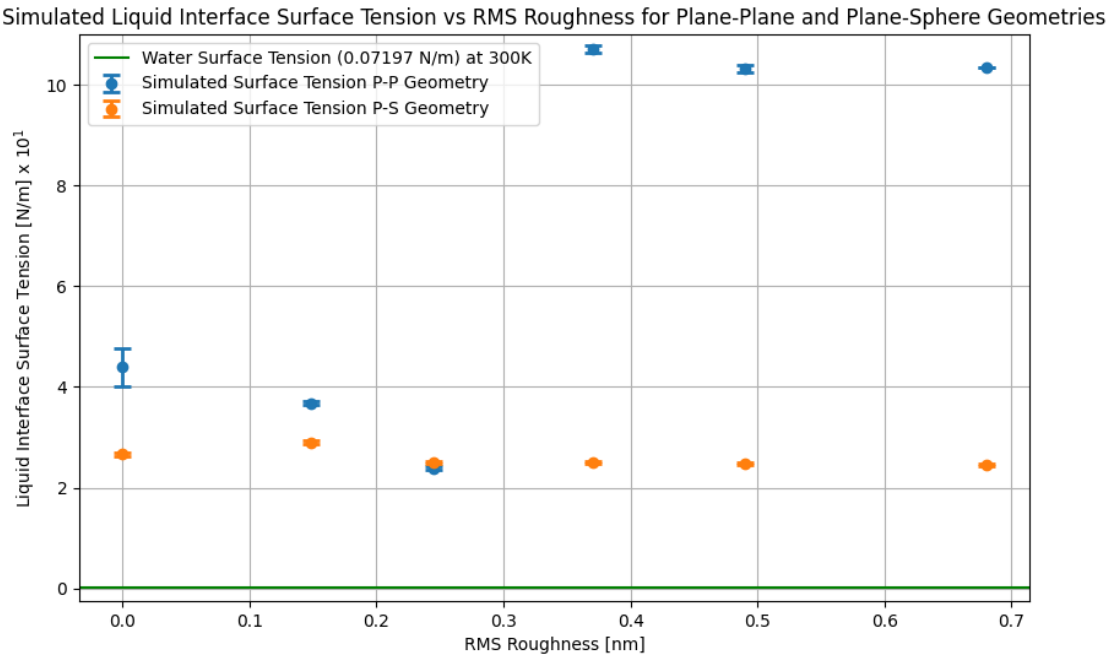

Figure 8: The simulated surface tension of water vs rms roughness in ambient conditions for two configurations. A horizontal line was introduced to illustrate the literature value (71.97 mN/m) [1].

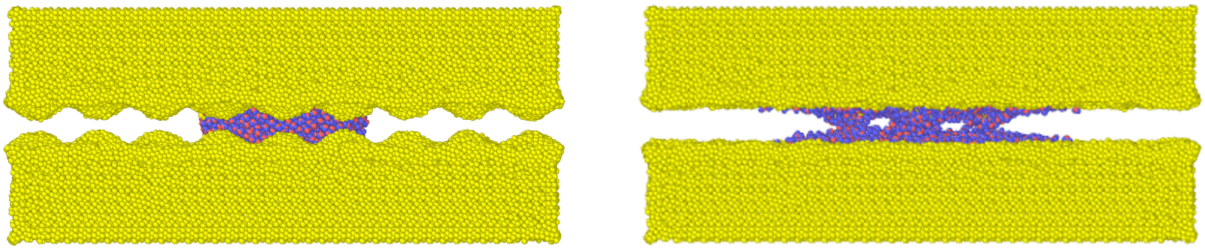

((a)) ((b))

Figure 9: (a) Snapshot of the plane-plane geometry in ambient conditions with 0.37nm rms roughness, right after the introduction of the components. (b) Final snapshot of an equilibrated ambient P-P system at 0.37nm rms roughness.

meniscus, were observed to assimilate and flatten into the surface throughout the simulation leading to a loss of rms roughness. This effect is most visible with bigger rms values (figure 9), and therefore, the true roughness values are not known. However, the influence is still spotted, as the formation of mini capillary bridges became more apparent with increasing rms (figure 9(b)). The pronounced effect occurred solely at rms greater or equal to 0.37nm for the plane-plane geometry and the sphere-plane geometry, indicating a complex interaction between the silicon surfaces and water molecules at the nano-scale. Further, in the S-P geometry, the total thickness of the capillary bridge (its inner radius r_1

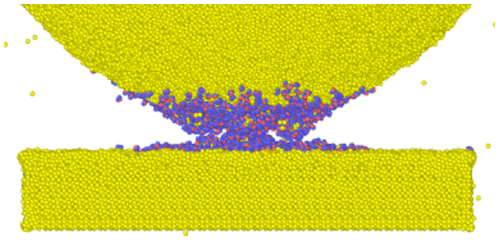

Figure 10: Final snapshot of an equilibrated ambient sphere-plane system at 0.49nm rms roughness.

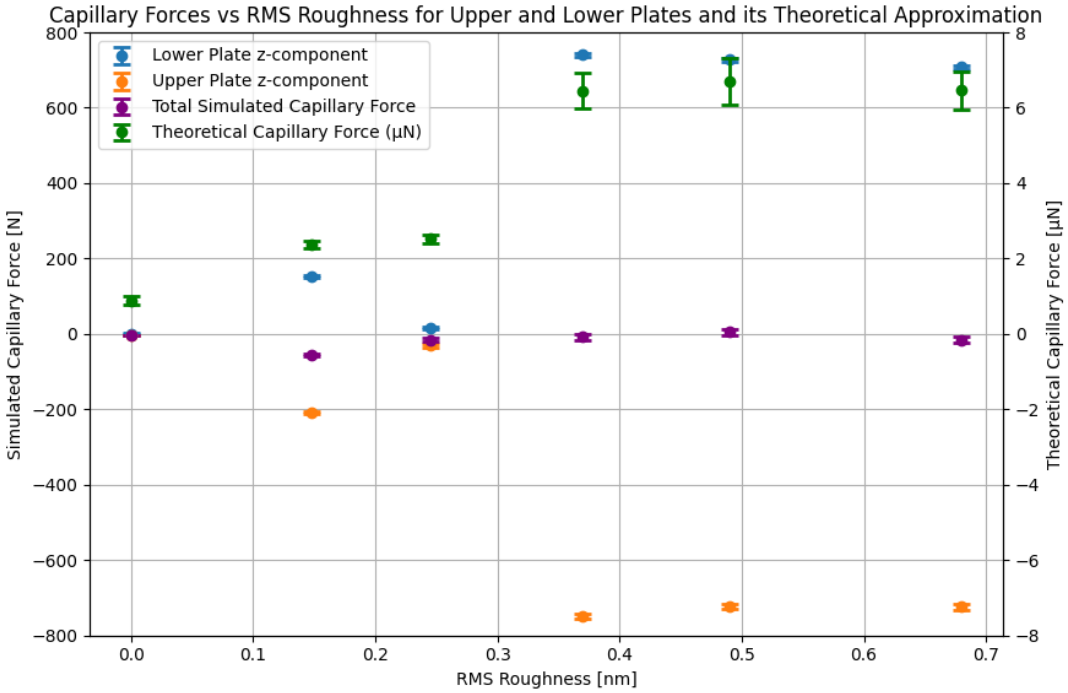

Figure 11: Simulated and theoretical capillary force values vs rms roughness in ambient conditions for the plane-plane geometry.

as shown in figure 4) increased with increasing roughness. For a rms roughness of 0.0 nm (perfectly flat), the most thin bridge was observed, with the majority of water molecules spreading across the surfaces.

All capillary forces can be seen in tables 3-6, with magnitudes ranging from 10^{-1} to 10^{3} N, including the simulated capillary force acting on both surfaces in the system, the total capillary force acting on the system and the theoretical prediction based on formulas 5 and 7 and the simulated liquid-gas surface tension. The capillary force in both configurations was observed to be attractive, with positive z-direction values for the lower silicon and negative for the upper silicon structures. The data points were plotted in figures 11-12.

For the P-P geometry, the force results of both plates have similar values but the opposite direction, indicating a balanced interaction. For rms 0.000-0.245nm they are in the range of approx. 200N. However, at rms 0.37nm, a sudden increase in their magnitude was observed

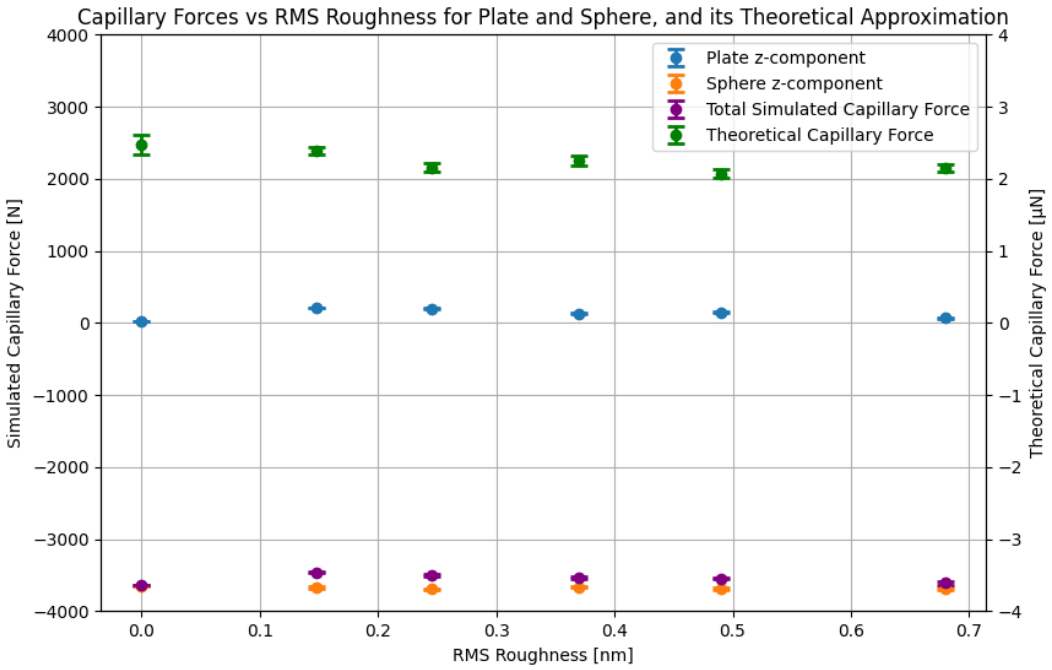

Figure 12: Simulated and theoretical capillary force values vs rms roughness in ambient conditions for the sphere-plane geometry.

due to the formation of the aforementioned capillary mini-bridges. This points to a step-like response of the magnitude of capillary forces to changes in surface roughness and the bridge geometry. Further, between rms values of 0.148 and 0.25nm, the components' force magnitude decreased without significant changes in the bridge geometry from snapshots.

In the SP geometry, the magnitude of the capillary forces is significantly larger compared to the plane-plane geometry by a factor of ten. This can be attributed to the greater capillary force component acting on the sphere, likely due to its geometric configuration and size (compared to the plate). On the contrary, the plate's force component exhibits a capillary force of the $10^1 - 10^2$ N magnitude, similar to the plane-plane system. Changes in the bridge geometry, such as increasing inner radius, were not reflected in the final capillary force values. Both the sphere component and the plane component values remain relatively stable, showing changes within the range of 50 and 200 N accordingly. This consistency highlights the robust nature of the sphere's interaction with varying roughness.

The total simulated capillary force acting on a system for the P-P geometry ranged between -15 and 5N, except -56.9939N at 0.48nm rms. The smallest magnitude overall was observed for the flat sample, indicating that the introduction of roughness to the perfectly smooth surface influenced the capillary forces in an enhancing manner. While, as the roughness increases further, the system remains relatively the same with slight variations. In contrast, the S-P geometry exhibits a greater magnitude of total simulated capillary force, primarily due to the sphere component. It suggests, that the sphere's geometry

RMS roughness [nm]	Capillary Force [N]	
	Lower Plate	Upper Plate
0.000	0.4785 ± 0.8578	-4.103 ± 1.0942
0.148	1.5261 ± 0.0214 $\times 10^2$	-2.0960 ± 0.02893 $\times 10^2$
0.245	1.4836 ± 0.2732 $\times 10^1$	-3.1166 ± 0.4015 $\times 10^1$
0.370	7.4103 ± 0.0453 $\times 10^2$	-7.4896 ± 0.0588 $\times 10^2$
0.490	7.2604 ± 0.0487 $\times 10^2$	-7.2169 ± 0.06619 $\times 10^2$
0.680	7.0816 ± 0.0509 $\times 10^2$	-7.2389 ± 0.0756 $\times 10^2$

Table 3: Final capillary force results acting upon each geometry component for varying rms roughness in plane-plane configuration and ambient conditions.

RMS roughness [nm]	Capillary Force [N]	
	Plate	Sphere
0.000	2.0064 ± 0.1713 $\times 10^1$	-3.6534 ± 0.0034 $\times 10^3$
0.148	2.1087 ± 0.04229 $\times 10^2$	-3.6719 ± 0.0088 $\times 10^3$
0.245	1.9522 ± 0.0604 $\times 10^2$	-3.6972 ± 0.0125$\times 10^3$
0.370	1.2686 ± 0.0605 $\times 10^2$	-3.6662 ± 0.0124 $\times 10^3$
0.490	1.4587 ± 0.0580 $\times 10^2$	-3.6902 ± 0.0127$\times 10^3$
0.680	7.2291 ± 0.8041 $\times 10^1$	-3.6834 ± 0.0173 $\times 10^3$

Table 4: Final capillary force results acting upon each geometry component for varying rms roughness in sphere-plane configuration and ambient conditions.

plays a crucial role in amplifying the capillary forces. Further, none of the values indicated specific increasing/decreasing trends, highlighting the complex nature of the interactions that require further detailed analysis.

The theoretical models for both geometries are in the μN scale, suggesting an issue in the magnitude of the simulated capillary forces. Theoretically, the P-P geometry demonstrated an overall step-like increasing trend in capillary force with increasing roughness. This trend aligned with the values of the individual plate components (except for 0.248nm rms) but not with the total force of the system. For the S-P geometry, the theoretical trend shows no specific decrease/increase in the values with oscillations between singular data points. It matches the relatively constant (small variation) simulated values.

4.2 Aqueous-Ambient Conditions

During the execution and troubleshooting of the simulation script, non-numerical pressure values were encountered, leading to the improper functioning of the simulation. Therefore, no values were obtained for the aqueous environment.

RMS roughness [nm]	Capillary Force [N]	
	Simulated	Theoretical $\times 10^{-6}$
0.000	-3.623±1.39	0.889 ± 0.104
0.148	-5.699±0.0359$\times 10^{1}$	2.362 ± 0.104
0.245	-1.633±0.486$\times 10^{1}$	2.523 ± 0.123
0.370	-7.931±7.421	6.452 ± 0.482
0.490	5.253±8.219	6.698 ± 0.612
0.680	-1.574±0.911$\times 10^{1}$	6.463±0.509

Table 5: Final total simulated and theoretical capillary force results for varying rms roughness in plane-plane configuration and ambient conditions.

RMS roughness [nm]	Capillary Force [N]	
	Simulated$\times 10^{3}$	Theoretical $\times 10^{-6}$
0.000	-3.633±0.004	2.473 ± 0.141
0.148	-3.461±0.009	2.385 ± 0.049
0.245	-3.501±0.013	2.156±0.064
0.370	-3.539±0.013	2.258±0.067
0.490	-3.544±0.014	2.071±0.053
0.680	-3.611±0.019	2.156±0.051

Table 6: Final total simulated and theoretical capillary force results for varying rms roughness in sphere-plane configuration and ambient conditions.

5 Discussion

5.1 Ambient Conditions

5.1.1 Surface Tension

The most significant outlier identified in the simulations was the greatly overestimated water's surface tension values with magnitudes of $10^1 - 10^2$ N/m. Since the literature value is in the order of 10^{-3}N/m [1], the results are strongly indicative of an issue with the simulation setup or parameters. Surface tension in molecular dynamics is highly sensitive to the force field parameters used to model intermolecular interactions. The σ and ϵ values in the Lennard Jones model (equation 11) for silicon-silicon and silicon-oxygen were selected based on a similar study done by Bryk et. al., that employed the same materials. However, it focused on studying the interactions between the liquid drop and the silicon surface [22]. Thus, the appropriate parameters might have varied while changing the system's configuration to a capillary force bridge with two solids. For σ, the arithmetic additivity of the parameters was chosen to estimate the σ_{Si-O}. The other rules (such as geometric or sixth power) could have been applied to observe their influence on the surface tension results [20]. Additionally, Bryk et. al. focused on varying the ϵ_{Si-O} value from 0.2786 to 0.6130 kcal/mole [22]. Hence, the upper boundary of the depth of the potential well, used in this investigation, might have had a significant influence on the results and greatly increased their value. Further, while the *.txt* file containing the SPC water model was modified to represent the DI water (no dissolved ions), the Lennard Jones parameters were not modified. Therefore, the lack of calibration of the DI water LJ coefficients could have enhanced the errors.

The surface tension values were obtained using the mechanical Irving Kirkwood model, which relies on a proper boundary conditions definition and the finite size effects [24],[26]. Due to time restraints, the simulations were done in the 27.5 nm-sized cube. Thus, a small simulation box could have introduced significant size-related effects, impacting the pressure tensors and, by proxy, the surface tension. A bigger simulation size should minimize these effects.

While a high surface tension of liquid would typically suggest a higher contact angle, the simultaneous decrease in CA, making the surface appear hydrophilic, can be attributed to several issues. In Young's equation (formula 9), the contact angle is influenced by the balance between surfaces and interfacial energies [14]. As γ_{lv} increases, the equation would suggest an increase in the angle as well, if γ_{sv} and γ_{sl} remain constant. However, the same sources of error that influenced the magnitude of water's surface tension, might have impacted the other energies as well. Thus, if γ_{sl} became significantly smaller or negative, while γ_{sv} increased in magnitude, the $\cos\theta$ would decrease appropriately. Therefore, the silicon surface tension and the interfacial surface tension should have been measured alongside the water's surface tension to obtain more interaction details. However, it is

important to note, that Young's equation is applied to a liquid drop on a surface (similar to the Bryk et. al. model [22]) and focuses on cohesive forces [14]. Thus, influential parameters from capillary forces are omitted in this model and the interaction obtained from the LAMMPS script is more complex.

5.1.2 Roughness

According to papers by Bakhshandehseraji et al [2], Zwol et al [5] and Sedighi et al [8]l, the increase in roughness should minimize the capillary force. However, this effect occurs starting from a specific roughness value. In Sedighi et al, the silicon carbide and borosilicate glass were employed. In this system, the capillary force remained relatively the same for $<$ 8nm and varied for 8-14nm plate + sphere rms roughness [8]. Bakhshandehseraji et al showed a similar trend with a great decrease above 8nm rms for gold-gold samples [2]. In Zwol et al, this drop in values occurred in the range of approx. 2-6 nm rms roughness of plate + sphere for gold-gold, gold-borosilicate, titanium-gold and gold-TiO2 [5]. Due to limited LAMMPS script optimization and time constraints, these rms roughness values were not studied. Therefore, a lack of any significant increasing/decreasing trends for the 0.00-1.36 nm rms roughness (the sum of the two components) aligns with the experimental data and confirms the rapid decrease threshold for two pure silicon surfaces in contact is somewhere above 1.36nm.

At greater rms roughness values, the formation of minibridges was observed. According to Bakhshandehseraji et al, on hydrophilic samples, this phenomenon should be responsible for the rapid decrease in the capillary force values [2]. Therefore, this suggests that the effective contact area between the asperities outweighs the increased wettability property. The lack of the system's response towards the formation of smaller bridges occurred most likely due to the size of the system. Since the scale was particularly small, the distances between the mini-bridges were in the range of approx. 0.3nm. Thus, considering the range of the forces, the bridges were still able to interact with each other and perform as a single capillary force bridge. Another variable that could have influenced this behaviour is the evenly distributed roughness. In real-life, the heights of singular asperities differ and do not resemble a 3D sine function [2]. Therefore, the amount of mini-capillary bridges formed might have been greater for the irregular surfaces used in the referenced studies.

During the addition of the roughness layer in the LAMMPS script, the simulations indicated the aforementioned loss of roughness, where the silicon atoms (with no DI water interactions) assimilated into the plate/sphere. This process increased the density of the solids while reducing the apparent roughness on the surface. Further, due to the loss of the outer layer, the total distance D also increased. Consequently, the obtained values were not representative of the initial roughness layers. Even with the SHAKE function applied, the layers could have been insufficiently rigid and bonded with the base plate/sphere model. On the other hand, the value of inserted roughness might have been too small to be

maintained in the equilibrated system, resulting in a non-representative simulation of the actual surface conditions.

For the theoretical models that employed the parameters obtained from the simulation, the increasing trend for the P-P and small magnitude oscillations for S-P geometry do not correspond accurately to its appropriate simulated behaviour. As mentioned before, the formulas (5-7) used to model the theoretical capillary forces apply for relatively flat surfaces. Therefore, the influence of roughness is only considered through the concept of surface tension. In a more rigorous approach, one must account for new formulas, taking into account roughness, whose behaviour is not limited solely to the cohesive forces acting on the liquid drop.

Further, equations 5-7 don't consider other complex parameters, such as the formation of mini-bridges (with an increase in the height of surface asperities) [2]. Hence, the step-like increase in the theoretical P-P configuration agrees with the assumptions from the Theory section. For the S-P geometry, as the roughness increased, the θ and ϕ angles did not change to a great extent. Consequently, it might be the origin of the small fluctuations and no specific (increasing/decreasing) trends visible. Further, due to the sphere's shape, the contact area between the liquid meniscus and the solid silicon does not increase in a step-like manner with roughness, as it does in P-P geometry. Thus, the spherical form ensures that any change in roughness only marginally influences the overall contact area. At the same time, the side-asperities influence the inner radius r_2 of the bridge by pushing the water molecules to the side.

While computing the theoretical results, most of the parameters from the equations were measured manually, including the scaling of lengths in each snapshot. Thus, variables such as contact angles and curvatures introduced potential human error and subjectivity in the determination of the manual errors. The assigned uncertainties might have been too small to account for the true error range and influence the theoretical model. Automatic software that optimizes the snapshot analysis would be a more suitable choice for more accurate measurements.

5.1.3 Simulation parameters

The final capillary force results for both simulated and theoretical models were computed to be significantly greater in magnitude than the experimental values. While the simulated results were $10^0 - 10^1$ N (P-P) and 10^3 N (S-P) order of magnitude and the theoretical values were 10^{-6} N of magnitude, the adhesion forces measured in Bakhshandehseraji et al show the range of $10^{-9} - 10^{-7}$ N [2]. The first major source of uncertainty, that influenced these results, is the aforementioned high surface tension for both systems. In both equations 5 and 7, surface tension plays a crucial role in the final capillary force value. Therefore, as the tension increased by an order of 10^3, the adhesion force should scale accordingly for the theoretical predictions. However, for the simulated values, this relationship proved to

be more complex, as the surface tension was not the sole contributor to this change in magnitude.

The reason behind the unusually high simulated capillary force values might stem from the code and its parameters themselves, as it has the same origin as the surface tension measurements. While constructing the system, silicon surfaces were modeled as rigid with the SHAKE function to remain in shape during the simulations. Thus, it may not have fully captured the dynamics of real surfaces, potentially affecting the accuracy of the capillary force measurements and increasing the magnitude of the capillary force. Additionally, the silicon surfaces were modeled as perfectly homogeneous with a consistent lattice structure. In real-life experimental conditions, solid surfaces contain various crystal facets, defects, and variations in the chemical composition, that lead to local changes in the contact angle and, by proxy, the capillary force [27]. Further, a modified SPC water model was employed as another simplification in the system. While effective, it is still a greatly simplified representation of water and doesn't account for all molecular interactions accurately [20].

As mentioned above, the size and length of the computations also greatly affected the accuracy of the model. Since the simulations had to be performed on a limited time scale, the number of time steps and the length of the equilibration and relaxation process were significantly cut. Thus, the system might have not been in its true equilibrium during the measurement process. The integration algorithm used in the script was Verlet, which is one of the simple and stable algorithms that integrate Newton's equations of motion in MD simulations [20]. It is well suited for long simulation times, which fits the scripts ran in this study. However, despite its stability, it requires relatively small timesteps to maintain accuracy [20]. Even though the timesteps applied in the code were in the 10^{-4} order of magnitude, this integration technique might simulate more accurate systems with even smaller timesteps. Further, to aid in the equilibration process, a Noose-Hoover NVT was employed. Under this specific ensemble, the non-equilibrium effects might dominate leading to transient and possibly non-physical forces in improperly equilibrated systems [20]. Thus, decreasing the accuracy of the final capillary force results.

Due to the simplification of choices, the study focused on pure silicon and DI water as its components. Therefore, limiting the applicability and comparisons of the findings with other materials or fluids. As mentioned above, the rms roughness threshold at which the change in capillary force shifts is dependent on the material used [5],[2],[8]. Therefore, for this investigation, it would be more beneficial to include (hydrophilic) materials utilized in the experimental research instead of simple and perfectly homogeneous structures.

5.2 Aqueous-Ambient Conditions

The LAMMPS script written for the NBCF bridge was based on a similar study, performed by Bird et al, which investigated the NBCF due to Ne gas bubbles between two Au plates submerged in liquid Ar for a simulation box of 65 $\times$ 35 $\times$ 35 nm [12]. However, due to

time constraints, the troubleshooting of the code was not successful with an output message "Non-Numeric Pressure". Thus, a couple of possible error origins should be explored.

While using the *delete_atoms* command and inserting the nitrogen gas into the cylinder, none of the existing atoms should still be located inside the region. Otherwise, overlapping atoms are created, which leads to extremely high repulsive forces [20]. Further, as mentioned in section 5.1, the pressure measurements are very sensitive to the input force parameters. The employed LJ parameters for the N-N interactions were used without the context of the NBCF bridge [23]. Therefore, they might be incorrect or non-optimized for these specific conditions. Similarly to the ambient conditions, the system might not have enough run time to reach the true equilibrium. Thus, in the case of a simulation with a significantly greater number of particles, the effects are enhanced and unrealistic pressure calculations that break the simulation might occur.

6 Conclusion

This study aimed to investigate the formation of the capillary force bridge due to DI water liquid meniscus and nitrogen nanobubbles under varying rms roughness conditions. The research was conducted employing the LAMMPS molecular dynamics software and focused on two system geometries: plane-plane (P-P) and sphere-plane (S-P). Despite the challenges encountered in equilibrating the aqueous conditions due to instability, several key insights were obtained from the simulations of the ambient environment. The findings highlighted significant discrepancies between the simulated, theoretical, and expected capillary forces, primarily due to issues with the simulation parameters and setup.

Under ambient conditions, the surface tension of water was vastly overestimated, with values ranging from 10^1 to 10^2 N/m, compared to the literature value of approximately 71.97 mN/m [1]. This discrepancy suggests possible errors such as incorrectly chosen Lennard-Jones parameters or inappropriate conditions for the Irving-Kirkwood model. The high surface tension values not only deviated from the literature but also impacted other related properties such as contact angle and the capillary forces in both theoretical and simulated models by proxy. Hence, making the naturally hydrophobic silicon surfaces appear as hydrophilic. This emphasizes the need for careful calibration of force field parameters and consideration of finite-size effects in simulations.

The variations in rms roughness in simulations revealed that the capillary force did not significantly change within the tested range of 0.00 to 1.36 nm total rms roughness (sum of two components). This aligns with experimental data suggesting a threshold roughness value beyond 1.36 nm for significant changes in pure silicon. The formation of mini-bridges at such small roughness values and the assimilation of the asperities into the base material during simulation indicate the complexity of accurately modeling rough surfaces and their interactions with fluids. For instance, the roughness layer assimilating into the silicon plate/sphere leads to an increase in density. Thus, reducing the apparent roughness, leading to non-representative values.

The theoretical models used to predict capillary forces displayed trends that partially agreed with the utilized formulas and the simulated behavior. For the plate-plate (P-P) geometry, the capillary force increased in a step-like function, confirming the increasing dependence of capillary forces on roughness for equation 5. In contrast, it did not correlate with the relatively constant simulated force output. This suggests, that the current models for P-P configuration may be more sensitive to roughness than anticipated. Conversely, for the sphere-plate (S-P) geometry, the theoretical models followed the experimental predictions more closely. Additionally, they demonstrated a more experimentally-accurate representation of the capillary forces, that remain unchanged with an increase in roughness for $<$0.68nm. However, both theoretical models focused solely on the roughness as a function of cohesive forces (surface tension). In turn, ignoring other complex parameters that were present in the simulated and experimental results. Thus, further proving the

limits of a theoretical approach for this subject. For more accurate in-depth research, new advanced formulas, that take into account roughness apart from its surface tension counterpart, are needed.

The final capillary force results for both simulated and theoretical models were significantly greater in magnitude than the experimental values. Simulated capillary forces were in the order of 10^0 to 10^1 N for P-P configurations and 10^3 N for S-P configurations, while the theoretical values had a magnitude of 10^{-6}N. On the contrary, the experimental adhesion forces of the gold-gold system were established by Bakhshandehseraj et al to be in the range of 10^{-9} to 10^{-7} N [2]. This discrepancy was attributed to the overestimated surface tension and limitations in the simulation setup, including the use of rigid, homogeneous silicon surfaces and a simplified DI water model.

The inability to equilibrate the NBCF environment in the aqueous conditions due to system instability points to further challenges in simulating such conditions. Future work should focus on improving the stability and accuracy of the simulations by refining force field parameters, increasing simulation box size, extending equilibration times, and incorporating more realistic surface and fluid models.

Overall, this study highlights the importance of parameter calibration and the limitations of both current molecular the dynamics simulations and theoretical formulas. Further research and optimization are necessary to bridge the gap between theoretical and experimental results, enabling more reliable predictions of capillary forces in various conditions.

7 Bibliography

[1] I. M. Hauner, A. Deblais, J. K. Beattie, H. Kellay **and** D. Bonn, "The dynamic surface tension of water," *J. Phys. Chem. Lett.*, **jourvol** 8, **pages** 1599–1603, 7 **march** 2017. DOI: https://doi.org/10.1021/acs.jpclett.7b00267.

[2] R. BakhshandehSeraji **and** G. Palasantzas, "Nanoscale-roughness influence on pull-off adhesion force in liquid and air," *Phys. Rev. E*, **jourvol** 108, **page** 054 801, 5 **november** 2023. DOI: 10.1103/PhysRevE.108.054801. **url**: https://link.aps.org/doi/10.1103/PhysRevE.108.054801.

[3] R. Michel, L. Poirier, Q. van Poelvoorde, J. Legagneux, M. Manassero **and** L. Corté, "Interfacial fluid transport is a key to hydrogel bioadhesion," *Proceedings of the National Academy of Sciences*, **jourvol** 116, **pages** 738–743, 3 **january** 2019. DOI: https://doi.org/10.1073/pnas.1813208116.

[4] W. Possart, *Adhestion, Current Research and Applications*. WILEY-VCH, 2005.

[5] P. J. van Zwol, G. Palasantzas **and** J. T. M. De Hosson, "Influence of roughness on capillary forces between hydrophilic surfaces," *Phys. Rev. E*, **jourvol** 78, **page** 031 606, 3 **september** 2008. DOI: 10.1103/PhysRevE.78.031606.

[6] A. G. P. Kottapalli, K. Tao, D. Sengupta **and** M. S. Triantafyllou, *Self-Powered and Soft Polymer MEMS/NEMS Devices*. Springer International Publishing, 2019, **pages** 1–30. DOI: 10.1007/978-3-030-05554-7.

[7] B. G. Abadi **and** M. Bahrami, "The effect of surface roughness on capillary rise in micro-grooves," *Sci. Rep.*, **jourvol** 12, **page** 14 867, **september** 2022. DOI: https://doi.org/10.1038/s41598-022-19111-w.

[8] M. Sedighi, V. B. Svetovoy **and** G. Palasantzas, "Capillary-force measurement on SiC surfaces," *Phys. Rev. E*, **jourvol** 93, **page** 062 803, **june** 2016. DOI: 10.1103/PhysRevE.93.062803.

[9] V. Svetovoy **and** G. Palasantzas, "Influence of surface roughness on dispersion forces," *Advances in Colloid and Interface Science*, **jourvol** 216, **pages** 1–19, 2015. DOI: https://doi.org/10.1016/j.cis.2014.11.001. **url**: https://www.sciencedirect.com/science/article/pii/S0001868614002814.

[10] H. Jürgen Butt **and** M. Kappl, "Normal capillary forces," *Advances in Colloid and Interface Science*, **jourvol** 146, **pages** 48–60, 1–2 **february** 2009. DOI: https://doi.org/10.1016/j.cis.2008.10.002.

[11] F. Xia, I. W. Rangelow **and** K. Youcef-Toumi, *Active Probe Atomic Force Microscopy*. Springer International Publishing, 2024. DOI: 10.1007/978-3-031-44233-9.

[12] E. Bird **and** Z. Liang, "Nanobubble capillary force between parallel plates," *Physics of Fluids*, **jourvol** 34, **page** 013 301, 1 **january** 2022. DOI: https://doi.org/10.1063/5.0075962.

[13] A. W. Foudas, R. I. Kosheleva, E. P. Favvos, M. Kostoglou, A. C. Mitropoilos **and** G. Z. Kyzas, "Fundamentals and applications of nanobubbles: A review," *Chemical*

Engineering Research and Design, **jourvol** 189, **pages** 64–86, 2023. DOI: https://doi.org/10.1016/j.cherd.2022.11.013.

[14] B. Arkles, "Hydrophobicity, hydrophilicity and silanes," *Paint Coatings Industry*, **october** 2006. **url**: https://www.gelest.com/wp-content/uploads/technical_library/HydrophobicityHydrophilicityandSilanes.pdf.

[15] A. Marmur, "The lotus effect: Superhydrophobicity and metastability.," *Langmuir*, **jourvol** 20, **pages** 3517–3519, 9 **april** 2004. DOI: 10.1021/la036369u.

[16] G. Neuss, *Chemistry for the IB diploma*. Oxford University Press, 2014, **pages** 54–58.

[17] R. Caenn, H. Darley **and** G. R. Gray, "Chapter 8 - the surface chemistry of drilling fluids," **in***Composition and Properties of Drilling and Completion Fluids (Seventh Edition)* Seventh Edition, Boston: Gulf Professional Publishing, 2017, **pages** 285–307, ISBN: 978-0-12-804751-4. DOI: https://doi.org/10.1016/B978-0-12-804751-4.00008-0. **url**: https://www.sciencedirect.com/science/article/pii/B9780128047514000080.

[18] K. Grundke, S. Michel, G. Knispel **and** A. Grundler, "Wettability of silicone and polyether impression materials: Characterization by surface tension and contact angle measurements," *Colloids and Surfaces A: Physicochemical and Engineering Aspects*, **jourvol** 317, **pages** 598–609, 1–3 2008. DOI: https://doi.org/10.1016/j.colsurfa.2007.11.046.

[19] R. Williams **and** A. M. Goodman, "Wetting of thin layers of sio2 by water," *Appl. Phys. Lett.*, **jourvol** 25, **pages** 531–532, 10 **november** 1974. DOI: https://doi.org/10.1063/1.1655297.

[20] LAMMPS, *Lammps documentation (17 apr 2024 version)*. **url**: https://docs.lammps.org/Manual.html.

[21] R. Harrison, J. Wathall, J. Harcet, M. T. Skoumal **and** L. Heinrichs, *Oxford IB Diploma Programme IB Mathematics: Analysis and Approaches, Higher Level*. Oxford University Press, 2019.

[22] P. Bryk, E. Korczeniewski, G. S. Szymański, P. Kowalczyk, K. Terpiłowski **and** A. P. Terzyk, "What is the value of water contact angle on silicon?" *Materials*, **jourvol** 13, **page** 1554, 7 **march** 2020. DOI: https://doi.org/10.3390/ma13071554.

[23] S. Wang, K. Hou **and** H. Heinz, "Accurate and compatible force fields for molecular oxygen, nitrogen, and hydrogen to simulate gases, electrolytes, and heterogeneous interfaces," *J. Chem. Theory Comput.*, **jourvol** 17, **pages** 5198–5213, 8 **july** 2021. DOI: https://doi.org/10.1021/acs.jctc.0c01132.

[24] E. Bird, J. Zhou **and** Z. Liang, "Coalescence speed of two equal-sized nanobubbles," *Phys. Rev. E*, **jourvol** 32, **page** 123 304, 12 **december** 2020. DOI: https://doi.org/10.1063/5.0030406.

[25] CODATA, *The 2022 codata recommended values of the fundamental physical constants*, [Online]. Available: https://physics.nist.gov/cgi-bin/cuu/Value?asil [Accessed 21.06.2024], 2022.

[26] E. R. Smith, D. M. Heyes **and** D. Dini, "Towards the irving-kirkwood limit of the mechanical stress tensor," *J. Chem. Phys.*, **jourvol** 146, 22 **june** 2017. DOI: https://doi.org/10.1063/1.4984834.

[27] E. Napetschnig, M. Schmid **and** P. Varga, "Pd, co and co–pd clusters on the ordered alumina film on nial(1 1 0): Contact angle, surface structure and composition," *Surface Science*, **jourvol** 601, 15 **august** 2007. DOI: https://doi.org/10.1016/j.susc.2007.05.047.

[28] N. Developers, *Numpy.std*, [Online]. Available: https://numpy.org/doc/stable/reference/generated/numpy.std.html [Accessed 24.06.2024].

[29] R. S. Figliola **and** D. E. Beasley, *Theory and Design for Mechanical Measurements, 6th Edition*. WILEY, 2015.

8 Appendix

All raw data can be accessed through **this link**. Additionally, the Google folder contains tables used for further calculations.

8.1 Error Analysis

The population's standard deviation formula used to obtain the error in the mean was the following

$$\sigma = \sqrt{\frac{\sum_i |a_i - \overline{a}|^2}{N}}, \tag{13}$$

where N is the size of the sample, a_i is one of the values from the sample and $\overline{a}$ is the mean value of the sample [28],[29]. To incorporate the assigned errors into the analysis, the partial derivative's error propagation approach was chosen

$$\Delta F_{cap}(x, y, z, ...) = \sqrt{(\frac{\partial F_{cap}}{\partial x}\Delta x)^2 + (\frac{\partial F_{cap}}{\partial y}\Delta y)^2 + (\frac{\partial F_{cap}}{\partial z}\Delta z)^2 + ...}, \tag{14}$$

where x, y, z are variables of F_{cap} [29].

8.2 Figures

Final snapshots of all runs can be seen in figures 13-22, 9, 10. The rest should be accessed through the aforementioned link. For figure 13, the total size of the simulation box is smaller by 10nm in the z-direction. Hence the distance between the plates seems bigger than in figures 14-17.

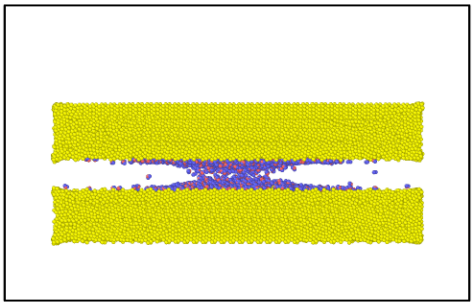

Figure 13: Final snapshot of an equilibrated ambient P-P system at 0.000nm rms roughness.

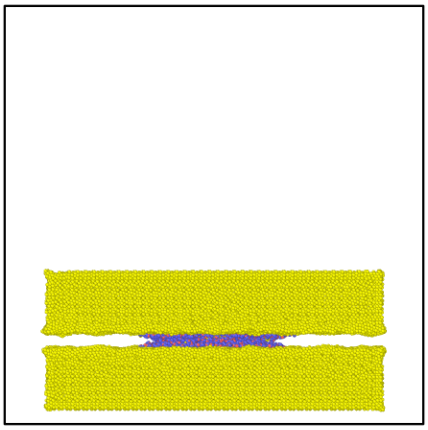

Figure 14: Final snapshot of an equilibrated ambient P-P system at 0.148nm rms roughness.

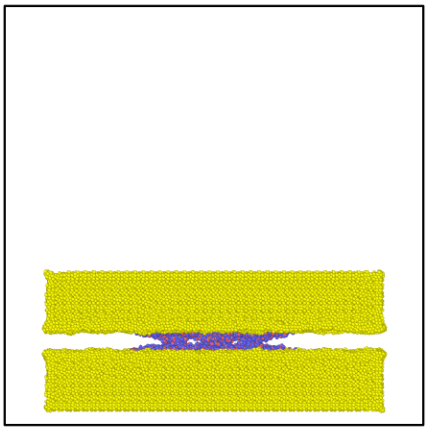

Figure 15: Final snapshot of an equilibrated ambient P-P system at 0.248nm rms roughness.

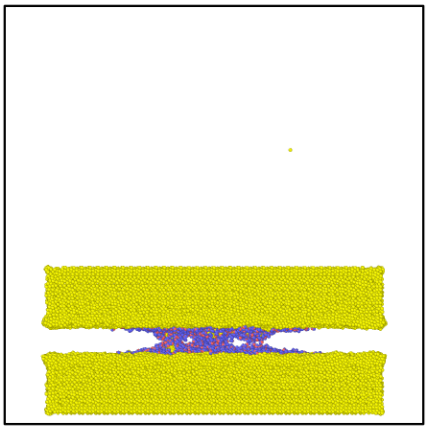

Figure 16: Final snapshot of an equilibrated ambient P-P system at 0.490nm rms roughness.

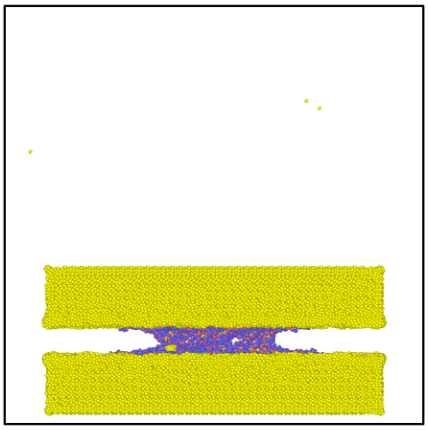

Figure 17: Final snapshot of an equilibrated ambient P-P system at 0.680nm rms roughness.

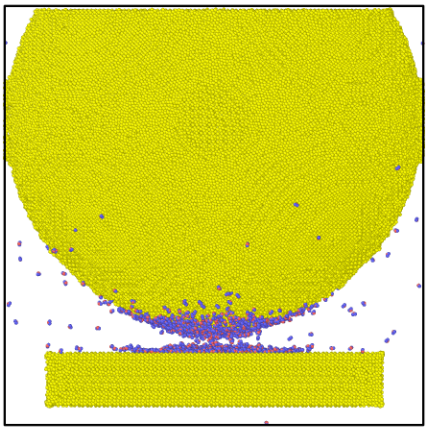

Figure 18: Final snapshot of an equilibrated ambient S-P system at 0.000nm rms roughness.

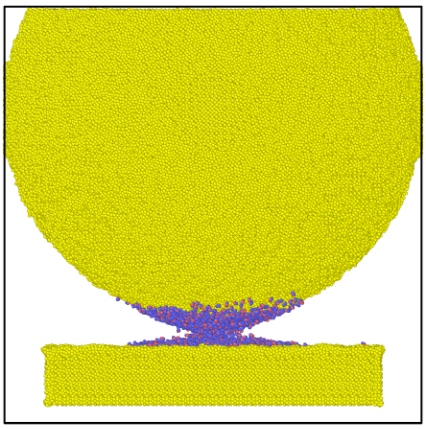

Figure 19: Final snapshot of an equilibrated ambient S-P system at 0.148nm rms roughness.

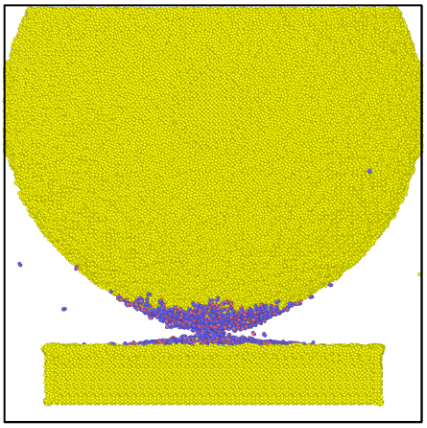

Figure 20: Final snapshot of an equilibrated ambient S-P system at 0.247nm rms roughness.

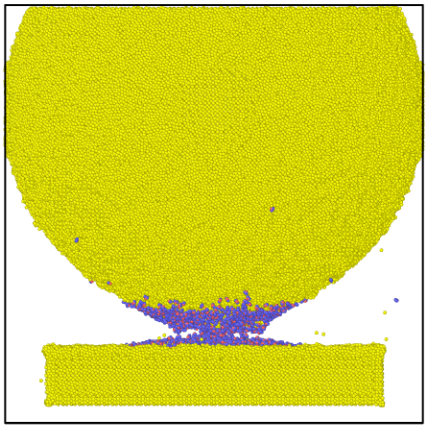

Figure 21: Final snapshot of an equilibrated ambient S-P system at 0.370nm rms roughness.

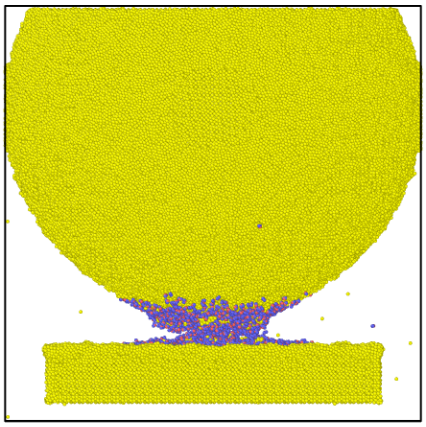

Figure 22: Final snapshot of an equilibrated ambient S-P system at 0.680nm rms roughness